

## Photochemistry and Thermal Chemistry in Polymeric Ceramic Precursors

Nabankur Dasgupta,<sup>#</sup> Kai Ito,<sup>#</sup> Thomas M. Linker,<sup>#</sup> Wataru Sugimoto,<sup>#</sup> Seyedmahmoud Mortazavi,<sup>#</sup> Rajiv K. Kalia, Aiichiro Nakano,\* Alexander T. Radosevich, Kohei Shimamura, Fuyuki Shimojo, Adri van Duin, and Priya Vashishta



Cite This: *J. Phys. Chem. Lett.* 2025, 16, 9874–9883



Read Online

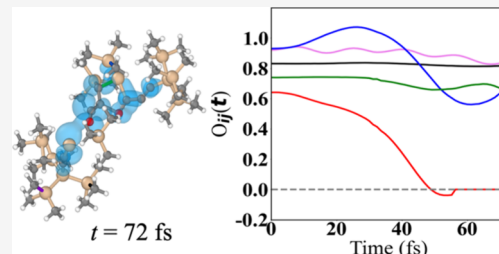
ACCESS |

Metrics & More

Article Recommendations

Supporting Information

**ABSTRACT:** While pyrolysis of polymeric precursors has gained attention for the additive manufacturing of ceramics, the high-temperature process is energy-inefficient and time-consuming. Recently, photochemistry has been suggested to reduce energy consumption and reaction time, but the microscopic mechanisms of such accelerated reactions remain elusive. Here, we reveal distinct photochemical and thermal reaction pathways at the initial stage of silicon–carbide ceramic formation from an acylsilane precursor, using a multiscale simulation approach that combines first-principles nonadiabatic and adiabatic quantum molecular dynamics simulations with semiempirical reactive molecular dynamics simulations. While photoexcitation causes scission of Si–C bonds within 100 fs driven by the localization of a photoexcited hole, the precursor remains stable at high temperatures up to 1800 K without photoexcitation. On longer time scales, we find thermal reaction pathways involving concerted motions of many atoms, including the formation of SiCO clusters, mainly resulting from oxygen of carbonyl carbon shifting and bonding with silicon. This microscopic understanding suggests synergistic use of photochemical and thermal pathways to design ultralow-energy and facile additive manufacturing of ceramics toward achieving a sustainable society.



Pyrolysis of polymeric precursors has gained much attention because of its crucial role in additive manufacturing of ceramics.<sup>1–3</sup> However, this high-temperature process consumes enormous energy, while requiring long processing time close to 24 h. Conventional methods to manufacture ceramics from constituent powders require bulk diffusion to transport matter from the grain interiors to grain boundaries. This condition imposes very high temperatures approaching two-thirds of the melting point of the material, thereby making the long-sought low-temperature ceramics processing substantially challenging, especially for metal carbides and other ultrahigh-temperature ceramic materials. Previously, researchers have seen some successes with field-assisted approaches such as applying microwave energy<sup>4</sup> and high-pressure processes,<sup>5</sup> which reduce densification times. However, intermediate temperature steps are still needed where unwanted residual spectator phases persist. Recently, photochemistry has been suggested instead to reduce both energy consumption and reaction time.<sup>6,7</sup> In these processes, high-intensity light interacts with a pre-ceramic polymer matrix to induce chemical reactions in the matrix that nucleates new or grows existing ceramic particles. A scientific hypothesis is that light modifies the energy landscape sufficiently due to electronic excitation, thereby opening more energy-efficient and rapid ceramic-forming reaction pathways.

A prototypical example of polymer-derived ceramics is silicon carbide (SiC) produced by the pyrolysis of polycarbosilanes. The Si–C composition in the microstructure of the ceramic primarily depends on the pyrolysis temperature and the precursor chemistry. Previous experiments have shown that a high ratio of silicon-to-carbon linkages in the ceramic is obtained from a pyrolysis temperature of 1000–1600 °C and low oxygen content in the precursor.<sup>8,9</sup> While the thermochemistries of such pyrolysis reactions have been well established by experiments<sup>10</sup> and atomistic molecular-dynamics (MD) simulations,<sup>11,12</sup> studies involving light-induced pyrolysis has been rather limited. Photochemical and thermal degradations lead to different reaction pathways toward ceramic formation.<sup>13,14</sup> Photochemistry is a nonadiabatic process in which electrons transition between excited states. Nonadiabatic quantum molecular dynamics (NAQMD) simulations serve as an important tool toward electronic and atomistic understanding of photochemical dynamics and reactivity from first principles.<sup>15–20</sup> On the other hand, conventional

Received: August 5, 2025

Revised: September 4, 2025

Accepted: September 5, 2025

thermal chemistry can be studied using adiabatic QMD simulations, in which electrons remain in the ground state.<sup>21–23</sup> For large systems for longer times, researchers instead employ semiempirical reactive molecular dynamics (RMD), as it incurs less computational cost. Especially, RMD simulations based on first-principles-informed ReaxFF force fields have been able to delineate the thermochemistry of a range of materials.<sup>11,24,25</sup>

For comparative study of photochemical and thermal reaction pathways at the initial stage of SiC ceramic formation, we perform first-principles NAQMD<sup>15–20</sup> and QMD<sup>21–23</sup> simulations of an acylsilane ( $\text{Si}_{14}\text{C}_{38}\text{H}_{90}\text{O}_2$ ) polymer precursor; see Figure 1. Acylsilanes are well-known photoreactive

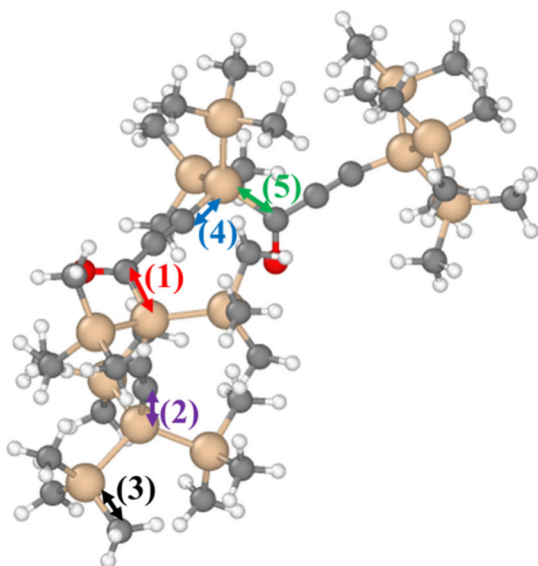


**Figure 1.** Structure of the thermally relaxed acylsilane precursor ( $\text{Si}_{14}\text{C}_{38}\text{H}_{90}\text{O}_2$ ) in a vacuum at temperature 300 K. Orange, gray, white, and red spheres represent Si, C, H, and O atoms, respectively. The selected five Si–C bonds (labeled 1 to 5) are distinguished by different colors.

functional groups,<sup>26</sup> with diverse applications including materials chemistry.<sup>27,28</sup> Upon UV irradiation,<sup>29</sup> they are known to undergo Si–C bond cleavage,<sup>30</sup> either via a Norrish type I mechanism to generate acyl and silyl radicals<sup>31</sup> or, alternatively, by a photoinduced 1,2-Brook rearrangement<sup>32</sup> to yield  $\alpha$ -siloxy carbenes.<sup>33</sup> The resulting reactive intermediates enable diverse transformations of potential relevance to ceramic formation.<sup>34</sup> For light-induced photochemical reaction pathways, we use NAQMD simulations (see Methods) that describe photoexcited dynamics of electrons and nuclei,<sup>15–20</sup> while thermal reaction pathways in conventional pyrolysis are studied using adiabatic QMD simulations (see Methods), in which electrons remain in the ground state.<sup>21–23</sup> The simulations are performed on a single acylsilane molecule containing 144 atoms in a box of  $30 \times 30 \times 30 \text{ \AA}^3$ .

**Photochemical NAQMD.** We first perform structural optimization of a representative acylsilane precursor,  $\text{Si}_{14}\text{C}_{38}\text{H}_{90}\text{O}_2$ , to obtain its minimum-energy atomic configuration; see Methods for details (Figure 1). Starting from the optimized atomic configuration, we then perform NAQMD simulations by exciting an electron. NAQMD describes photoexcitation dynamics involving electrons and nuclei from first principles in the framework of time-dependent density

functional theory (TDDFT)<sup>35</sup> and nonadiabatic coupling between electrons and nuclei.<sup>15–20</sup> We selected specific molecular orbitals (MOs) for electronic excitation. Using an intense light with photon energy exceeding the 4 eV (ultraviolet range), an electron is excited from the highest occupied MO (HOMO) to an unoccupied MO. Of particular interest in photochemistry is its enhancement by nanoparticles, which involves photoionization.<sup>36,37</sup> To mimic such a process, we selected a delocalized unoccupied MO spanning the entire molecule. To identify suitable unoccupied MO candidates, we calculate the participation number (PN)<sup>38</sup> that quantifies spatial delocalization of wave functions; see eq 1 in Methods. Table 1 shows the PNs for unoccupied MOs and their

**Table 1. Participation Numbers (PNs) for HOMO and Unoccupied MOs up to LUMO+25 in the Relaxed Structure and Corresponding Differences in the Eigenenergy ( $\Delta E$ ) from the HOMO Energy, Both Shown in Figure 1<sup>a</sup>**

Molecular orbital	PN	$\Delta E$ (eV)
HOMO	6.4240	0
LUMO	5.0580	1.7966
LUMO+1	5.0030	2.0083
LUMO+2	12.3700	3.3863
LUMO+3	16.5800	3.7403
LUMO+4	17.5200	3.8303
LUMO+5	16.1300	3.8923
LUMO+6	39.5100	3.9423
LUMO+7	11.4100	4.0383
LUMO+8	25.5400	4.1593
LUMO+9	26.2500	4.1853
LUMO+10	27.2700	4.2093
LUMO+11	38.9600	4.2483
LUMO+12	37.6200	4.3153
LUMO+13	49.4300	4.3693
<b>LUMO+14</b>	<b>51.5000</b>	<b>4.4493</b>
LUMO+15	27.5300	4.4923
<b>LUMO+16</b>	<b>52.0600</b>	<b>4.5253</b>
LUMO+17	20.2000	4.5483
LUMO+18	43.5900	4.5983
LUMO+19	45.3800	4.6263
LUMO+20	23.0900	4.6413
LUMO+21	37.9800	4.6663
LUMO+22	49.7500	4.6753
LUMO+23	47.1500	4.7163
LUMO+24	26.4400	4.7403
LUMO+25	57.8200	4.8033

<sup>a</sup>Excited electronic orbitals in three different NAQMD simulations are shown in boldface.

eigenenergy differences from that of HOMO, where  $\text{LUMO}+n$  denotes the  $n$ th lowest unoccupied MO (LUMO) but one. The unoccupied MO with the largest PN is LUMO+25, corresponding to an eigenenergy difference of approximately 4.8 eV. The second and third highest PNs are LUMO+16 and LUMO+14 with an eigenenergy difference of around 4.5 eV. We therefore choose three different target MOs for electronic excitation from HOMO, i.e., LUMO+14, LUMO+16, and LUMO+25. We observe similar dynamics of electronic excitation for all three cases. Below, we present results for LUMO+14, while those for LUMO+16 and LUMO+25 are presented in the Supporting Information.

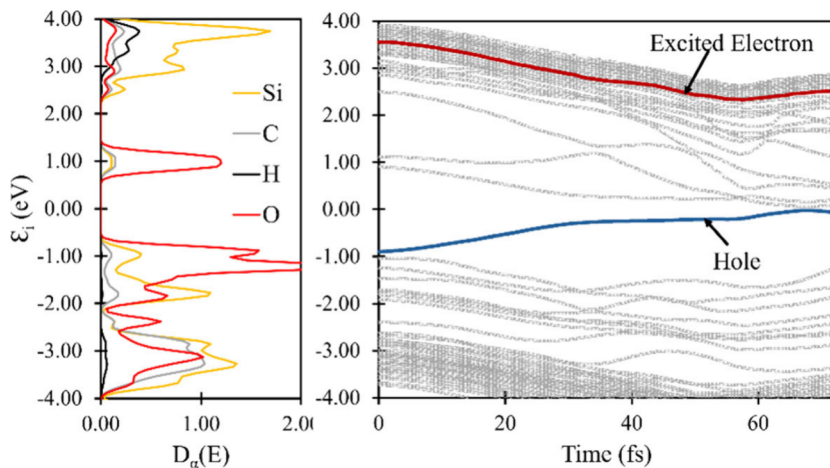


**Figure 2.** (Left) Partial electronic densities of states  $D_\alpha(E)$  for the relaxed structure obtained from single-point calculation after optimization, where orange, gray, black, and red curves are, respectively, for species  $\alpha = \text{Si}, \text{C}, \text{H}$ , and  $\text{O}$ . (Right) Time evolution of electronic eigenenergies during the NAQMD simulation. The blue and red curves indicate those of the hole and excited electron, respectively.

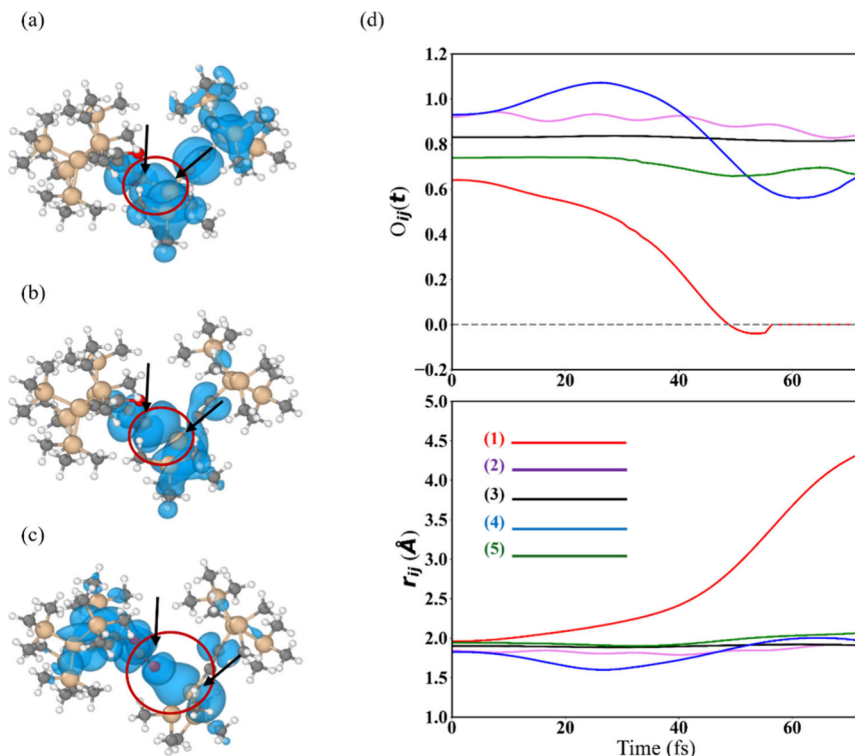


**Figure 3.** Snapshots of the dissociation process of a Si–C ( $\text{Si}1\text{--C}1$ ) bond of acylsilane precursor at  $t = 0$  (a), 48 (b), and 72 fs (c). The isosurface of the hole charge density with 0.0002 au is shown in light blue. The red circles are guides for the eyes. (d) Bond overlap population ( $O_{ij}(t)$ , top) and lengths ( $r_{ij}(t)$ , bottom) of the five selected Si–C bonds. The line colors in the panel correspond to the bond colors in Figure 1.

The left panel of Figure 2 shows the partial density of states  $D_\alpha(E)$  for the relaxed structure shown in Figure 1. The orange, gray, black, and red curves are for species  $\alpha = \text{Si}, \text{C}, \text{H}$ , and  $\text{O}$ , respectively. The right panel of Figure 2 shows the time evolution of electronic eigenenergies  $\epsilon_i$  ( $i$  is the orbital index) during NAQMD simulation, in which the hole and excited electron levels are marked by blue and red curves. At  $t = 0$ , the hole exists in the HOMO, which resides on O and Si atoms (mainly O atoms). Since the molecule has only two O atoms, the HOMO is spatially localized around the O atoms. It is also understood from  $D_\alpha(E)$  that LUMO and LUMO+1 are also localized around O atoms. The corresponding PNs of HOMO,

LUMO, and LUMO+1 are small (<10; see Table 1), reflecting spatial localization of these wave functions. On the other hand, the excited electrons at  $t = 0$  (i.e., LUMO+14) are composed of atomic orbitals of all four chemical species (mainly Si atoms), which reflect the unlocalized nature of the wave function. After  $t > 0$ , the hole remains in HOMO beyond 60 fs, while the excited electron gradually transfers from LUMO+14 to lower-lying MOs. The latter represents decay of the electronic excitation energy assisted by atomic motions through nonadiabatic coupling, thus transferring energy from electrons to atoms.<sup>39</sup> Another notable process is the decreasing gap between the HOMO and LUMO energies as a function of

time until they become very close at  $t = 68$  fs. Because the electronic excitation energy is transferred to atoms as described above, the resulting molecular deformation tends to close the HOMO–LUMO gap, as was observed in other molecular systems.<sup>40,41</sup>

Panels a–c of Figure 3 show snapshots of acylsilane precursor at  $t = 0$ , 48, and 72 fs, respectively, in the NAQMD simulation, where isosurfaces of the hole charge density are colored light blue. An important feature of this NAQMD simulation is the dissociation of Si–C bonds near the spatial position where the holes are localized. This Si–C bond (circled red in Figure 3a) is the one labeled 1 in Figure 1, which we denote as Si1–C1. Figure 3d shows the time evolution of the bond overlap population  $O_{ij}(t)$  of Si–C bonds using Mulliken analysis,<sup>42,43</sup> along with that of the corresponding bond lengths  $r_{ij}(t)$  between Si and C atoms.  $O_{ij}(t)$  and  $r_{ij}(t)$  for the other four Si–C bonds (labeled 2–5) are also shown for comparison. At  $t = 0$ ,  $O_{\text{Si1-C1}}(t)$  and  $r_{\text{Si1-C1}}(t)$  are 0.65 and 2.0 Å, respectively, which are comparable to those of the other Si–C bonds. However,  $O_{\text{Si1-C1}}(t)$  and  $r_{\text{Si1-C1}}(t)$  subsequently undergo noticeable changes.  $O_{\text{Si1-C1}}(t)$  is reduced to half, 0.35, at  $t = 36$  fs, and then reached almost zero at  $t = 48$  fs (see Figure 3b); i.e., the Si1–C1 bond is dissociated.  $r_{\text{Si1-C1}}(t)$  monotonically increases after 48 fs. Considering that the hole is localized near this Si–C bond, we can conclude that the dissociation is caused by a photochemical effect. Similar bond scission due to a localized hole has been observed in polymers such as polyethylene.<sup>44</sup> Bond-overlap and bond-length distributions for different Si–C bonds within the molecule are in good agreement among all three NAQMD simulations (Figure S3 in the Supporting Information). The hole localization leading to the dissociation of the particular Si–C bond in acylsilane is found to occur around the same time in all three cases.

We next examined the possibility that photothermal effects contributed to the Si–C scission observed above. To do so, we monitor the time evolution of temperature during the NAQMD simulation (Figure 4). The temperature increases

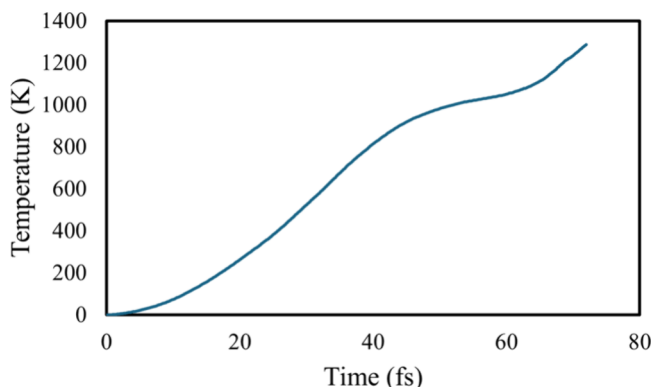
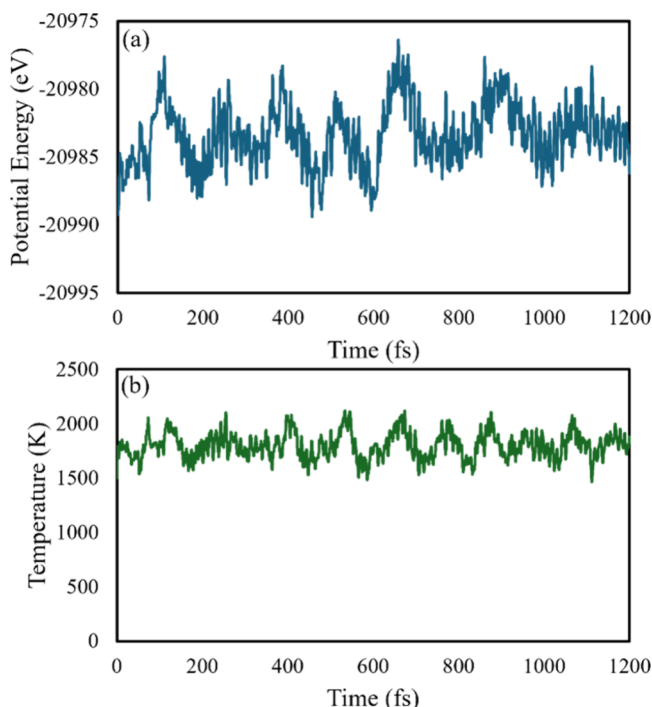


**Figure 4.** Time evolution of temperature during the NAQMD simulation.

rapidly from the initial 300 K to over 1200 K during the simulation. Thus, we cannot rule out the possibility that this high temperature caused the observed Si–C bond scission. From the time at which hole localization occurs ( $t \sim 36$  fs), we obtain the photothermal temperature reaching close to 700 K. To understand the photothermal behavior of Si–C scissions, we study the same polymer at different temperatures.

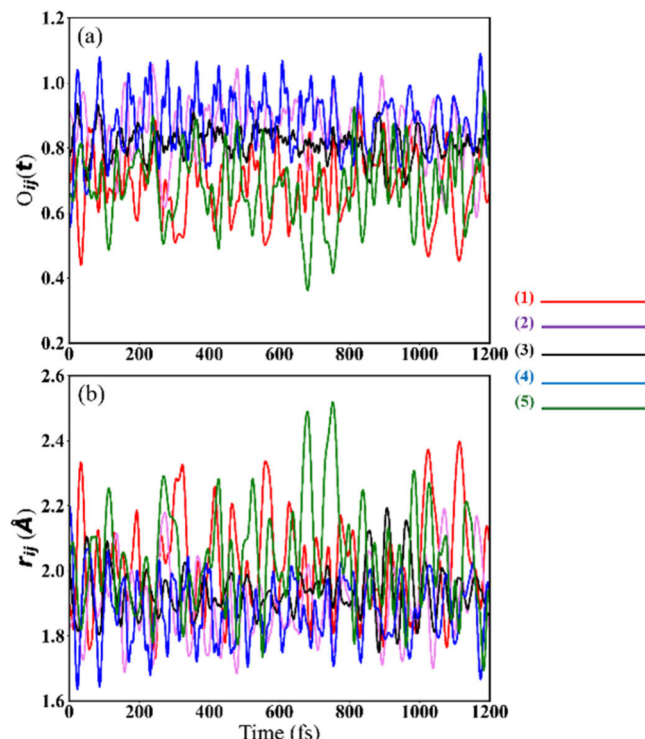
**Thermal chemistry: Adiabatic QMD.** To study purely thermal chemistry in contrast to the photochemistry studied by the above NAQMD simulation, we perform an adiabatic QMD simulation, in which electrons stay in the ground state. We use the same initial atomic configuration as in the NAQMD simulation (i.e., the one shown in Figure 1). According to the bond overlap population in Figure 3d, the strength of the Si–C bond in the NAQMD simulation decreased by approximately half at 36 fs. The photothermal temperature reaches close to 700 K at this time. Therefore, if the photothermal effect is dominant, a similar reduction in bond strength should be observable in a QMD simulation conducted at 700 K or higher. Therefore, we perform adiabatic QMD simulations in the canonical (NVT) ensemble at 300, 600, 900, 1200, 1500, and 1800 K for 1200 fs, which is an order-of-magnitude longer than the NAQMD simulation.

Figure 5 shows the time evolution of the potential energy and temperature during the adiabatic QMD simulation at 1800



**Figure 5.** Time evolution of the potential energy (a) and temperature (b) during adiabatic QMD simulation in the canonical ensemble at 1800 K.

K, which confirms that the system is in a steady state at the highest temperature. Figure 6 shows the  $O_{ij}(t)$  and  $r_{ij}(t)$  of the five selected Si–C bonds shown in Figure 1. While both  $O_{ij}(t)$  and  $r_{ij}(t)$  fluctuate rapidly, no bond dissociation is observed during the entire adiabatic QMD simulation. We do not see any significant change in the bond distance of the particular Si–C bond that is dissociated upon electronic excitation. Therefore, we conclude that elevated temperature due to photoexcitation alone cannot explain the photoinduced bond scission observed in the NAQMD simulation and that the Si–C bond dissociation is dominated by the photochemical effect (i.e., photoinduced change of the energy landscape) rather than the thermal effect. However, one of the striking observations from the bond overlaps and distances is that the silicon linked to the carbonyl carbon (i.e., those labeled 1



**Figure 6.** Time evolution of the (a) bond overlap populations ( $O_{ij}(t)$ ) and (b) bond lengths ( $r_{ij}(t)$ ) of the five selected Si–C bonds during QMD simulation in the canonical ensemble at 1800 K. The line colors correspond to the bond colors in Figure 1.

and 5) shows the largest fluctuation compared with the other Si–C bonds. This indicates that 1.2 ps may be too short to observe any significant reactive events like bond dissociation in an adiabatic QMD simulation. Experiments on the synthesis and degradation of acylsilane polymers indeed found these Si–C bonds to be the most reactive in nature.<sup>34</sup> This bond can break both photochemically (as seen) and thermally, initiating the pyrolysis process.

**ReaxFF RMD Simulations.** While the above nonadiabatic and adiabatic QMD simulations have revealed drastically different photochemical and thermal reaction pathways at the initial stage, high-temperature thermal reactions at longer times likely involve concerted motions of many atoms due to the higher kinetic energy. However, this is beyond the reach of first-principles QMD simulations. To complement the adiabatic QMD simulations and explore longer-time chemical reactivity at high temperatures, we employ reactive molecular dynamics (RMD) simulations of 20 acylsilane molecules (Figure 7) using a reactive force field (ReaxFF).

We track the dissociation behavior of the five most reactive Si–C bonds, as identified in Figure 1, during simulations at four different temperatures between 1250 and 2000 K. The number of intact bonds for each of these five Si–C pairs is recorded throughout the simulation, and the results are presented in Figure 8a–d respectively for 1250, 1500, 1750, and 2000 K. Among these, the Si–C bond labeled as “bond 3”, corresponding to the silicon atom linked to a methyl group, is found to be the most thermally unstable, exhibiting the fastest dissociation rate, especially at elevated temperatures. While some Si–C bonds remain intact even after 500 ps of RMD at 1250 and 1500 K, nearly all are dissociated at high temperatures of 1750 and 2000 K and beyond 1 ns for all

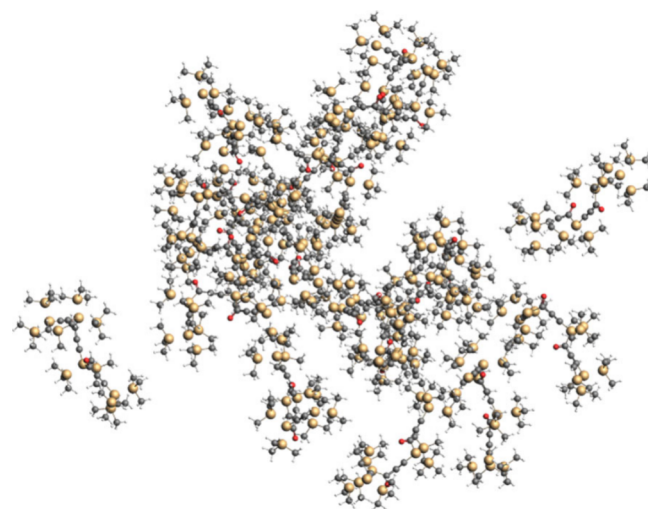


**Figure 7.** Initial structure consisting of 20 acylsilane molecules ( $\text{Si}_{14}\text{C}_{38}\text{H}_{90}\text{O}_2$ ) randomly placed in a simulation box. Orange, gray, white, and red spheres represent Si, C, H, and O atoms, respectively.

temperatures (see Figure 8). The rate of bond dissociation (for bonds 1–5) also increases with increased temperature, as seen in Figure 8. At high temperatures, bonds dissociate and rearrange to form new structures, which are the elementary blocks for novel materials. To provide a broader perspective on the extent of Si–C bond dissociation, Figure 9 shows the total number of Si–C bonds normalized to an initial count of 100 bonds for each temperature. At 2000 K, nearly complete dissociation of the Si–C bonds occurs by 1 ns. These results demonstrate that the rate of Si–C bond dissociation increases with temperature, confirming the thermally activated nature of the decomposition process. Bonds 1 and 5, which have Si linked to carbonyl carbons, dissociate and release oxygens from the carbonyl carbons. These oxygens react to give other radicals during pyrolysis. One such instance has been observed in our RMD simulations at 2000 K as seen in Figure 10. The oxygen attached to the carbonyl carbon (C1) rearranges by moving close to silicon atoms (Si1 and Si2), and a substitution reaction is seen to occur by carbon moving from one silicon atom (Si1) to another (Si2). The old Si bond with the carbonyl carbon atom (Si1–C) breaks and a new Si–C bond (Si2–C) forms along with a new Si–O bond (Si1–O) as seen in Figure 10. Such rearrangements lead to the formation of SiCO linkages on pyrolysis. We observed small clusters of SiCO within the system at a high temperature of 2000 K. Figure 11 is a representative depiction of the formation of pre-ceramic SiCO from the pyrolysis of acylsilane polymers.

As the pyrolysis progresses, small pre-ceramic clusters such as those shown above continue to nucleate and grow. At high temperatures, the nucleation of small clusters is influenced by factors like increased kinetic energy of molecules. Apart from pre-ceramic formation from pyrolysis, we also observe massive gaseous products, such as lower hydrocarbons and hydrogen. From our simulations, the main products observed are  $\text{CH}_4$  and  $\text{H}_2$  molecules along with large SiCO clusters. The evolution of  $\text{CH}_4$  and  $\text{H}_2$  molecules throughout the simulations is shown in Figure 12. Formation of both  $\text{CH}_4$  and  $\text{H}_2$  is found to increase with the temperature, indicating higher dissociation and radicalization. The separation of gases from the pyrolysis reactions can accelerate the formation of pre-ceramic formation as seen in previous experiments.

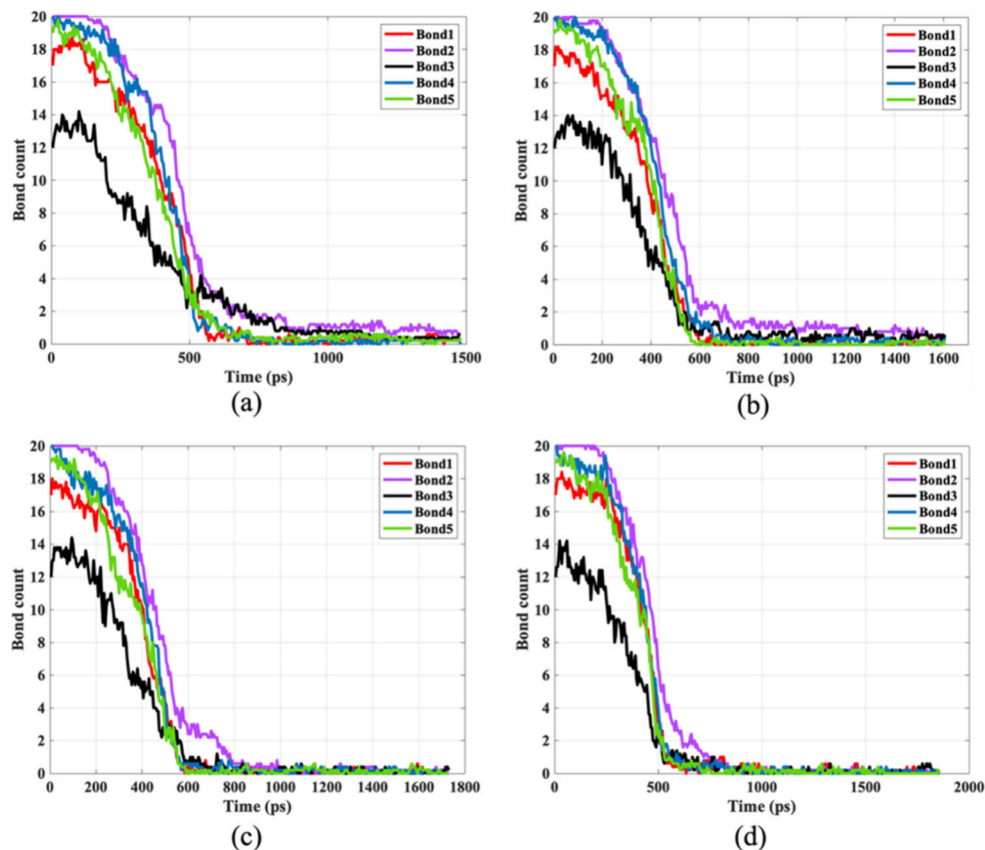


**Figure 8.** Time evolution of 5 selected Si–C bond counts at temperatures of 1250 (a), 1500 (b), 1750 (c), and 2000 K (d).

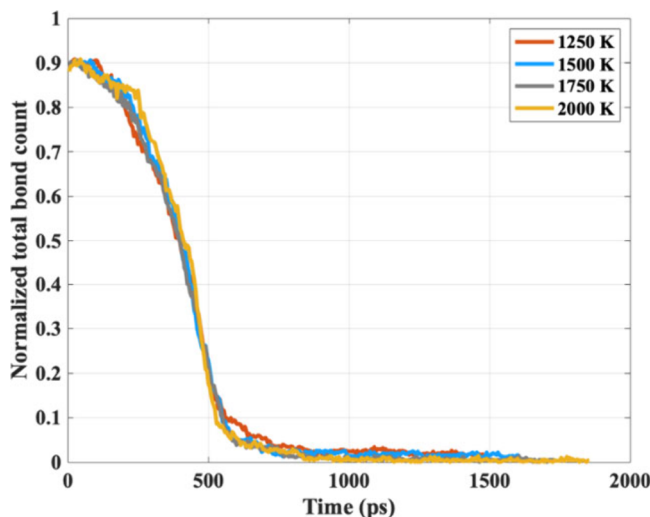


**Figure 9.** Time evolution of the total number of Si–C bonds normalized to the total initial bond count at four different temperatures.

In summary, we have performed first-principles nonadiabatic and adiabatic QMD simulations to reveal distinct photochemical and thermal reaction pathways at the initial stage of silicon–carbide ceramic formation from the acylsilane precursor. While photoexcitation caused scission of Si–C bonds within 72 fs at zero temperature, the precursor was stable at high temperatures below 1800 K without photoexcitation. The electronic mechanism underlying the photochemical SiC scission was found to be the localization of a

photoexcited hole at the SiC bond. In contrast to the localized bond scission in such low-temperature photochemistry, RMD simulations revealed thermal reaction pathways involving concerted motions of many atoms at higher temperatures and longer time. Most notably, we observed the formation of SiCO clusters, mainly resulting from the oxygen of carbonyl carbon shifting and bonding with silicon. Such microscopic understanding suggests the synergistic use of photochemical and thermal pathways to design ultralow-energy and rapid additive manufacturing of ceramics. For example, photochemistry can be used for the scission of targeted chemical bonds by tuning photon energy and pulse shape,<sup>45</sup> which in turn accelerates downstream thermal chemistry at moderate temperatures to reduce both energy consumption and reaction time for additive manufacturing of ceramics. In practice, pairing photochemical initiation with controlled thermal postprocessing could allow an additive manufacturing strategy that lowers the peak applied temperature, shortens hold times, and enables spatially selective conversion for functionally graded parts by patterned irradiation. In situ experiments based on ultrafast pump–probe,<sup>46,47</sup> FTIR/XPS,<sup>48</sup> and TGA-MS techniques that correlate photoinduced cluster formation and macroscopic ceramic yield would be instrumental in establishing an empirical validation of this approach.

## METHODS

**QMD and NAQMD Methods.** Quantum molecular dynamics (QMD)<sup>21–23</sup> follows the trajectories of all atoms while computing interatomic forces quantum mechanically from first principles in the framework of density functional theory (DFT).<sup>49,50</sup> In an adiabatic QMD based on the Born–

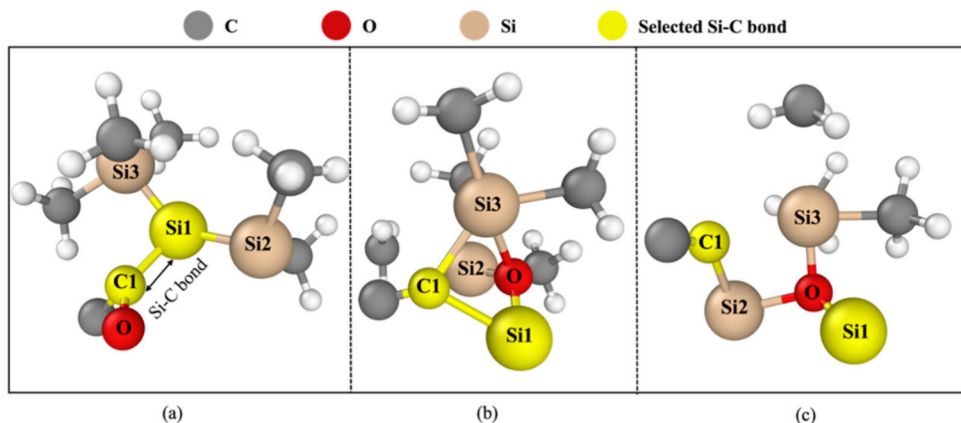


**Figure 10.** Si–C bond breakage pathway. (a) Initial structure, (b) oxygen atom transfers from carbon atom to silicon atoms, and (c) Si–C bond completely breaks.

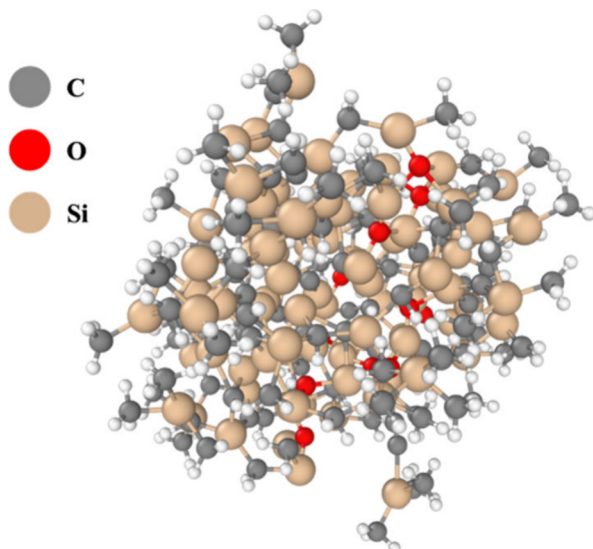


**Figure 11.** Structure of a SiCO cluster formed during the RMD simulation.

Oppenheimer approximation, electrons remain in their ground state, thereby describing thermal reactions that do not involve electronic excitation. On the other hand, nonadiabatic quantum molecular dynamics (NAQMD)<sup>15–20</sup> describes

electronic excitations in the framework of time-dependent density functional theory (TDDFT),<sup>35</sup> thus allowing the study of photochemistry.

For both QMD and NAQMD simulations, the electronic states are calculated using the projector-augmented wave (PAW) method,<sup>51</sup> where projector functions are generated for  $1s^1$  for H,  $2s^2 2p^2$  for C,  $2s^2 2p^4$  for O, and  $3s^2 3p^2 3d^0$  for Si atoms. The generalized gradient approximation (GGA) is used for the exchange–correlation functional.<sup>52</sup> The plane-wave cutoff energies are set as 30 Ry for wave functions and 300 Ry for the electron density. Brillouin zone sampling is performed at the  $\Gamma$  point. Our QXMD code<sup>53</sup> implements a series of methods to efficiently compute interatomic forces incorporating electronic excitations.<sup>54</sup>

**System Preparation.** We place an acylsilane precursor ( $\text{Si}_{14}\text{C}_{38}\text{H}_{90}\text{O}_2$ ) in a cubic supercell with a length of 30 Å, and structural optimization using a quasi-Newton method was performed for 600 steps to prepare an initial atomic configuration of subsequent QMD simulations. We perform a single-point electronic-structure calculation to obtain the density of states and participation numbers for different molecular orbitals.

**NAQMD Simulation of Photochemistry.** NAQMD simulations are performed in the microcanonical (NVE) ensemble for 72 fs with a unit time step of  $\Delta t = 0.24$  fs. We

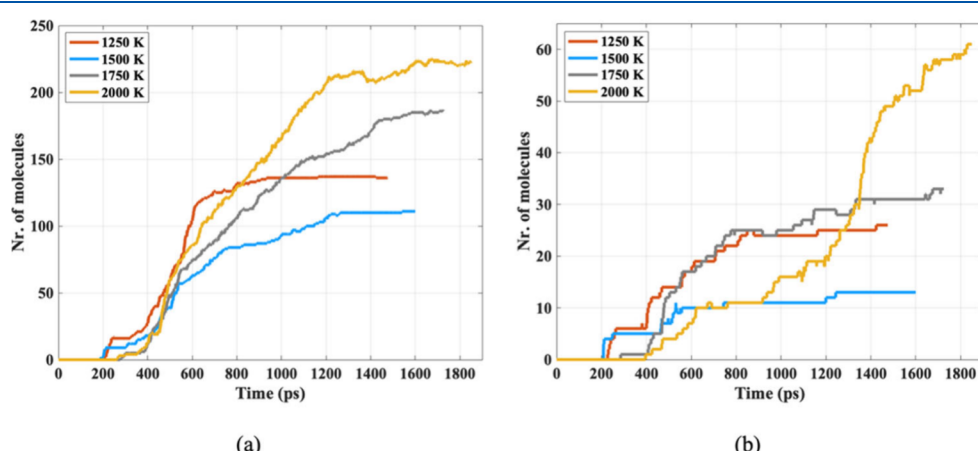


**Figure 12.** Number of (a) CH<sub>4</sub> and (b) H<sub>2</sub> molecules formed during simulation at four different temperatures.

consider one electron excitation from HOMO to LUMO+14, LUMO+16, and LUMO+25.

**QMD Simulation of Thermal Chemistry.** Using the same initial atomic coordinates and velocities of the NAQMD simulation, QMD simulations are performed in the canonical (*NVT*) ensemble at temperatures 300, 600, 900, 1200, 1500, and 1800 K for 1200 fs with  $\Delta t = 0.24$  fs.

**Participation Numbers.** Using the existing probability  $p_{i\lambda}$  of the  $\lambda$ th wave function on the  $i$ th atom, the participation number  $\pi_\lambda$  for the wave function is calculated as follows:<sup>38</sup>

$$\pi_\lambda = \frac{1}{\sum_i^N p_{i\lambda}^2} \quad (1)$$

where  $N$  is the number of atoms of the system. The existing probabilities are calculated by Mulliken analysis.<sup>42,43</sup>

**ReaxFF Force Field.** ReaxFF is a general bond order-dependent force field that provides accurate descriptions of bond formation and bond breaking in a wide range of materials and chemical systems.<sup>24</sup> ReaxFF has a low computational cost compared to quantum mechanical (QM) methods. This makes ReaxFF capable of simulating large systems over a long time. By using the ReaxFF method, there is no need to predefine the reactive sites and reaction pathways, and as a result, the outputs are unbiased by user assumptions. ReaxFF parameters are trained against QM data describing both reaction energies and reaction barriers, typically using a successive single-parameter search optimization technique.<sup>55</sup> Similar to other empirical nonreactive force fields,<sup>56</sup> the energy of the system in ReaxFF is partitioned into partial energy contributions:

$$E_{\text{system}} = E_{\text{bond}} + E_{\text{over}} + E_{\text{under}} + E_{\text{val}} + E_{\text{lp}} + E_{\text{tors}} \\ + E_{\text{vdWaals}} + E_{\text{Coulomb}} \quad (2)$$

where partial energies are associated with the bond, overcoordination, undercoordination, valence angle, lone pair, torsion, van der Waals, and Coulomb interactions, respectively. We employed C/H/Si/O ReaxFF force field by Soria et al.<sup>57</sup> to investigate the thermal chemistry involved in the formation of SiC ceramics. The ReaxFF force field parameters are given in the Supporting Information. Given the similarity in chemical systems between this study and that of ref 57, this force field is well-suited for our simulations.

**RMD Simulation of High-Temperature and Long-Time Thermal Chemistry.** The initial geometry was constructed by placing 20 acylsilane molecules in a cubic simulation box measuring  $60 \times 60 \times 60 \text{ \AA}^3$  with an intermolecular spacing of 2.5 Å between each molecule as shown in Figure 7. The system was first energy minimized and then equilibrated in two stages. In the first stage, we employed an isothermal–isobaric (*NPT*) ensemble (constant number of atoms, pressure, and temperature) at room pressure and temperature (pressure of 1 atm and temperature of 300 K) for 50 ps to allow the system to reach its equilibrium density. The Berendsen barostat and thermostat<sup>58</sup> were used to control the pressure and temperature, with damping constants of 100 and 10 fs, respectively. In the second stage, the temperature increased from 300 K to target values of 1250, 1500, 1750, and 2000 K at a heating rate of 2 K/ps under the *NVT* ensemble, where the number of atoms ( $N$ ), volume ( $V$ ), and temperature ( $T$ ) were kept constant. Following the equilibration, *NVT* simulations were conducted at different temperatures of 1250, 1500, 1750, and 2000 K. The temperature was regulated using

the Berendsen thermostat with a damping constant of 50 fs. A time step of 0.25 fs was used throughout the simulations. Each simulation was performed for a total duration of 1 ns. Periodic boundary conditions were employed in all three directions. To ensure statistically meaningful results, we performed an ensemble of five independent simulations, each initialized with a different random configuration. The results were averaged across the ensemble.

## ASSOCIATED CONTENT

### Supporting Information

The Supporting Information is available free of charge at <https://pubs.acs.org/doi/10.1021/acs.jpclett.5c02429>.

Additional simulation results and force field including additional NAQMD simulation results (Figures S1–S6) and ReaxFF force-field parameters (PDF)

Video S1 showing NAQMD simulation (MP4)

## AUTHOR INFORMATION

### Corresponding Author

Aiichiro Nakano – Collaboratory for Advanced Computing and Simulation, University of Southern California, Los Angeles, California 90089-0242, United States;  [orcid.org/0000-0003-3228-3896](https://orcid.org/0000-0003-3228-3896); Email: [anakano@usc.edu](mailto:anakano@usc.edu)

### Authors

Nabankur Dasgupta – Collaboratory for Advanced Computing and Simulation, University of Southern California, Los Angeles, California 90089-0242, United States

Kai Ito – Department of Physics, Kumamoto University, Kumamoto 860-8555, Japan

Thomas M. Linker – Stanford PULSE Institute, SLAC National Accelerator Laboratory, Menlo Park, California 94025, United States;  [orcid.org/0000-0002-0504-4876](https://orcid.org/0000-0002-0504-4876)

Wataru Sugimoto – Department of Physics, Kumamoto University, Kumamoto 860-8555, Japan

Seyedmahmoud Mortazavi – Department of Mechanical Engineering, Pennsylvania State University, University Park, Pennsylvania 16802, United States

Rajiv K. Kalia – Collaboratory for Advanced Computing and Simulation, University of Southern California, Los Angeles, California 90089-0242, United States

Alexander T. Radosevich – Department of Chemistry, Massachusetts Institute of Technology, Cambridge, Massachusetts 02139, United States;  [orcid.org/0000-0002-5373-7343](https://orcid.org/0000-0002-5373-7343)

Kohei Shimamura – Department of Physics, Kumamoto University, Kumamoto 860-8555, Japan;  [orcid.org/0000-0003-3235-2599](https://orcid.org/0000-0003-3235-2599)

Fuyuki Shimojo – Department of Physics, Kumamoto University, Kumamoto 860-8555, Japan;  [orcid.org/0000-0002-4025-0069](https://orcid.org/0000-0002-4025-0069)

Adri van Duin – Department of Mechanical Engineering, Pennsylvania State University, University Park, Pennsylvania 16802, United States;  [orcid.org/0000-0002-3478-4945](https://orcid.org/0000-0002-3478-4945)

Priya Vashishta – Collaboratory for Advanced Computing and Simulation, University of Southern California, Los Angeles, California 90089-0242, United States;  [orcid.org/0000-0003-4683-429X](https://orcid.org/0000-0003-4683-429X)

Complete contact information is available at:

<https://pubs.acs.org/doi/10.1021/acs.jpclett.5c02429>

**Author Contributions**

#N.D., K.I., T.M.L., W.S., and S.M. contributed equally to this work. N.D., K.I., T.M.L., and W.S. performed NAQMD and QMD simulations. S.M. performed RMD simulations. A.N., K.S., and F.S. provided NAQMD and QMD simulation and analysis techniques. A.T.R. provided the molecular structure. A.v.D. provided RMD simulation techniques. R.K.K., A.N., P.V., and A.v.D. designed the research. All authors discussed and prepared the manuscript.

**Notes**

The authors declare no competing financial interest.

**ACKNOWLEDGMENTS**

This work was supported by Office of Naval Research through a Multi-University Research Initiative (MURI) Grant N00014-24-1-2313. Simulations were performed at the Center for Advanced Research Computing of the University of Southern California. Computing was also provided by the U.S. DOE INCITE and Aurora ESP Programs.

**REFERENCES**

- (1) Eckel, Z. C.; Zhou, C.; Martin, J. H.; Jacobsen, A. J.; Carter, W. B.; Schaefler, T. A. Additive manufacturing of polymer-derived ceramics. *Science* **2016**, *351* (6268), 58–62.
- (2) O'Masta, M. R.; Stonkevitch, E.; Porter, K. A.; Bui, P. P.; Eckel, Z. C.; Schaefler, T. A. Additive manufacturing of polymer-derived ceramic matrix composites. *J. Am. Ceram. Soc.* **2020**, *103* (12), 6712–6723.
- (3) Chaudhary, R. P.; Parameswaran, C.; Idrees, M.; Rasaki, A. S.; Liu, C.; Chen, Z.; Colombo, P. Additive manufacturing of polymer-derived ceramics: materials, technologies, properties and potential applications. *Prog. Mater. Sci.* **2022**, *128*, 100969.
- (4) Bhandavat, R.; Kuhn, W.; Mansfield, E.; Lehman, J.; Singh, G. Synthesis of polymer-derived ceramic Si(B)CN-carbon nanotube composite by microwave-induced interfacial polarization. *ACS Appl. Mater. Interf.* **2012**, *4* (1), 11–16.
- (5) Wang, X.; Peng, W.; Hu, Y.; Yang, M.; Han, D.; Ma, C.; Lin, Y.; Wang, H.; Zhang, R.; Zhang, Z.; Shao, G. High-pressure synthesis of fully dense polymer-derived SiCN ceramics: structural evolution and mechanical properties. *J. Euro. Ceram. Soc.* **2024**, *44* (15), 116760.
- (6) Kimura, S.; Tanushi, A.; Kusamoto, T.; Kochi, S.; Sato, T.; Nishihara, H. A luminescent organic radical with two pyridyl groups: high photostability and dual stimuli-responsive properties, with theoretical analyses of photophysical processes. *Chem. Sci.* **2018**, *9* (7), 1996–2007.
- (7) Bao, C.; Zhu, L.; Lin, Q.; Tian, H. Building biomedical materials using photochemical bond cleavage. *Adv. Mater.* **2015**, *27* (10), 1647–1662.
- (8) Li, Y.-L.; Kroke, E.; Riedel, R.; Fasel, C.; Gervais, C.; Babonneau, F. Thermal cross-linking and pyrolytic conversion of poly(ureamethylvinyl)silazanes to silicon-based ceramics. *App. Organometal. Chem.* **2001**, *15* (10), 820–832.
- (9) Narisawa, M.; Funabiki, F.; Iwase, A.; Wakai, F.; Hosono, H. Effects of atmospheric composition on the molecular structure of synthesized silicon oxycarbides. *J. Am. Ceram. Soc.* **2015**, *98* (10), 3373–3380.
- (10) Hackbarth, H. G.; Key, T. S.; Ackley, B. J.; Opletal, G.; Rawal, A.; Gallington, L.; Yang, Y.; Thomsen, L.; Dickerson, M. B.; Pruyt, T. L.; Bedford, N. M. Uncovering atomic-scale polymer-to-ceramic transformations in SiC polymer derived ceramics from polycarbosilanes. *J. Euro. Ceram. Soc.* **2024**, *44* (4), 1932–1945.
- (11) Naserifar, S.; Goddard, W. A.; Liu, L.; Tsotsis, T. T.; Sahimi, M. Toward a process-based molecular model of SiC membranes. 2. reactive dynamics simulation of the pyrolysis of polymer precursor to form amorphous SiC. *J. Phys. Chem. C* **2013**, *117* (7), 3320–3329.
- (12) Ponomarev, I.; van Duin, A. C. T.; Kroll, P. Reactive force field for simulations of the pyrolysis of polysiloxanes into silicon oxycarbide ceramics. *J. Phys. Chem. C* **2019**, *123* (27), 16804–16812.
- (13) Billingham, N. C. Degradation and stabilization of polymers. In *Materials Science and Technology: A Comprehensive Treatment, The Classic Edition*; Wiley: 2013; pp 469–507. DOI: 10.1002/9783527603978.mst0412.
- (14) de Sainte Claire, P. Degradation of PEO in the solid state: a theoretical kinetic model. *Macromol.* **2009**, *42* (10), 3469–3482.
- (15) Craig, C. F.; Duncan, W. R.; Prezhdo, O. V. Trajectory surface hopping in the time-dependent Kohn-Sham approach for electron-nuclear dynamics. *Phys. Rev. Lett.* **2005**, *95* (16), 163001.
- (16) Tully, J. C. Perspective: nonadiabatic dynamics theory. *J. Chem. Phys.* **2012**, *137* (22), 22A301.
- (17) Shimojo, F.; Ohmura, S.; Mou, W.; Kalia, R. K.; Nakano, A.; Vashishta, P. Large nonadiabatic quantum molecular dynamics simulations on parallel computers. *Comput. Phys. Commun.* **2013**, *184* (1), 1–8.
- (18) Lin, M. F.; Kochat, V.; Krishnamoorthy, A.; Bassman Oftelie, L.; Weninger, C.; Zheng, Q.; Zhang, X.; Apte, A.; Tiwary, C. S.; Shen, X. Z.; Li, R. K.; Kalia, R.; Ajayan, P.; Nakano, A.; Vashishta, P.; Shimojo, F.; Wang, X. J.; Fritz, D. M.; Bergmann, U. Ultrafast non-radiative dynamics of atomically thin MoSe<sub>2</sub>. *Nat. Commun.* **2017**, *8*, 1745.
- (19) Tung, I.; Krishnamoorthy, A.; Sadasivam, S.; Zhou, H.; Zhang, Q.; Seyler, K. L.; Clark, G.; Mannebach, E. M.; Nyby, C.; Ernst, F.; Zhu, D.; Glownia, J. M.; Kozina, M. E.; Song, S.; Nelson, S.; Kumazoe, H.; Shimojo, F.; Kalia, R. K.; Vashishta, P.; Darancet, P.; Heinz, T. F.; Nakano, A.; Xu, X.; Lindenberg, A. M.; Wen, H. Anisotropic structural dynamics of monolayer crystals revealed by femtosecond surface x-ray scattering. *Nat. Photon.* **2019**, *13*, 425–430.
- (20) Linker, T.; Nomura, K.; Aditya, A.; Fukushima, S.; Kalia, R. K.; Krishnamoorthy, A.; Nakano, A.; Rajak, P.; Shimmura, K.; Shimojo, F.; Vashishta, P. Exploring far-from-equilibrium ultrafast polarization control in ferroelectric oxides with excited-state neural network quantum molecular dynamics. *Sci. Adv.* **2022**, *8* (12), No. eabk2625.
- (21) Car, R.; Parrinello, M. Unified approach for molecular-dynamics and density-functional theory. *Phys. Rev. Lett.* **1985**, *55* (22), 2471–2474.
- (22) Payne, M. C.; Teter, M. P.; Allan, D. C.; Arias, T. A.; Joannopoulos, J. D. Iterative minimization techniques for ab initio total-energy calculations - molecular-dynamics and conjugate gradients. *Rev. Mod. Phys.* **1992**, *64* (4), 1045–1097.
- (23) Shimojo, F.; Hattori, S.; Kalia, R. K.; Kunaseth, M.; Mou, W.; Nakano, A.; Nomura, K.-i.; Ohmura, S.; Rajak, P.; Shimmura, K.; Vashishta, P. A divide-conquer-recombine algorithmic paradigm for multiscale materials modeling. *J. Chem. Phys.* **2014**, *140* (18), 18A529.
- (24) Senftle, T. P.; Hong, S.; Islam, M. M.; Kylasa, S. B.; Zheng, Y.; Shin, Y. K.; Junkermeier, C.; Engel-Herbert, R.; Janik, M. J.; Aktulga, H. M.; Verstraelen, T.; Grama, A.; van Duin, A. C. T. The ReaxFF reactive force-field: development, applications and future directions. *npj Comput. Mater.* **2016**, *2*, 15011.
- (25) Dasgupta, N.; Mao, Q.; van Duin, A. C. T. Computationally guided synthesis of carbon coated mesoporous silica materials. *Carbon* **2024**, *221*, 118891.
- (26) Zhang, H.-J.; Priebeinow, D. L.; Bolm, C. Acylsilanes: valuable organosilicon reagents in organic synthesis. *Chem. Soc. Rev.* **2013**, *42* (21), 8540–8571.
- (27) Huang, B.; Wei, M.; Vargo, E.; Qian, Y.; Xu, T.; Toste, F. D. Backbone-photodegradable polymers by incorporating acylsilane monomers via ring-opening metathesis polymerization. *J. Am. Chem. Soc.* **2021**, *143* (43), 17920–17925.
- (28) Ratushnyy, M.; Zhukhovitskiy, A. V. Polymer skeletal editing via anionic Brook rearrangements. *J. Am. Chem. Soc.* **2021**, *143* (43), 17931–17936.
- (29) Glotz, G.; Puschmann, S.; Haas, M.; Gescheidt, G. Direct detection of photo-induced reactions by IR: from Brook rearrangement to photo-catalysis. *Photochem. Photobio. Sci.* **2023**, *22* (7), 1683–1693.

- (30) Porter, N. A.; Iloff, P. M., Jr. Application of chemically induced dynamic nuclear polarization to a study of acylsilane photolysis. *J. Am. Chem. Soc.* **1974**, *96* (19), 6200–6202.
- (31) Brook, A. G.; Duff, J. M. Optical stability of asymmetric silyl radicals. *J. Am. Chem. Soc.* **1969**, *91* (8), 2118–2119.
- (32) Brook, A. G.; Harris, J. W.; Lennon, J.; El Sheikh, M. Relatively stable silaethylenes. Photolysis of acylpolysilanes. *J. Am. Chem. Soc.* **1979**, *101* (1), 83–95.
- (33) Priebebenow, D. L. Insights into the stability of siloxy carbene intermediates and their corresponding oxocarbenium ions. *J. Org. Chem.* **2019**, *84* (18), 11813–11822.
- (34) Wang, X.; Liu, F. X.; Li, Y.; Yan, Z.; Qiang, Q.; Rong, Z.-Q. Recent advances in the synthesis of acylsilanes. *ChemCatChem.* **2020**, *12* (20), 5022–5033.
- (35) Runge, E.; Gross, E. K. U. Density-functional theory for time-dependent systems. *Phys. Rev. Lett.* **1984**, *52* (12), 997–1000.
- (36) Dagar, R.; Zhang, W.; Rosenberger, P.; Linker, T. M.; Sousa-Castillo, A.; Neuhaus, M.; Mitra, S.; Biswas, S.; Feinberg, A.; Summers, A. M.; Nakano, A.; Vashishta, P.; Shimojo, F.; Wu, J.; Vera, C. C.; Maier, S. A.; Cortés, E.; Bergues, B.; Kling, M. F. Tracking surface charge dynamics on single nanoparticles. *Sci. Adv.* **2024**, *10* (32), No. eadp1890.
- (37) Linker, T. M.; Dagar, R.; Feinberg, A.; Sahel-Schackis, S.; Nomura, K.; Nakano, A.; Shimojo, F.; Vashishta, P.; Bergmann, U.; Kling, M. F.; Summers, A. M. Catalysis in extreme field environments: a case study of strongly Ionized SiO<sub>2</sub> nanoparticle surfaces. *J. Am. Chem. Soc.* **2024**, *146* (40), 27563–27570.
- (38) Mou, W.; Hattori, S.; Rajak, P.; Shimojo, F.; Nakano, A. Nanoscopic mechanisms of singlet fission in amorphous molecular solid. *Appl. Phys. Lett.* **2013**, *102* (17), 173301.
- (39) Brown, E.; Sheng, C.; Shimamura, K.; Shimojo, F.; Nakano, A. Enhanced charge recombination due to surfaces and twin defects in GaAs nanostructures. *J. Appl. Phys.* **2015**, *117* (5), 054307.
- (40) Riad Manaa, M. Shear-induced metallization of triaminotrinitrobenzene crystals. *Appl. Phys. Lett.* **2003**, *83* (7), 1352–1354.
- (41) Shimamura, K.; Misawa, M.; Li, Y.; Kalia, R. K.; Nakano, A.; Shimojo, F.; Vashishta, P. A crossover in anisotropic nano-mechanochemistry of van der Waals crystals. *Appl. Phys. Lett.* **2015**, *107* (23), 231903.
- (42) Mulliken, R. S. Electronic population analysis on LCAO-MO molecular wave functions. 1. *J. Chem. Phys.* **1955**, *23* (10), 1833–1840.
- (43) Shimojo, F.; Nakano, A.; Kalia, R. K.; Vashishta, P. Electronic processes in fast thermite chemical reactions: a first-principles molecular dynamics study. *Phys. Rev. E* **2008**, *77* (6), 066103.
- (44) Kumazoe, H.; Fukushima, S.; Tiwari, S.; Kim, C.; Huan, T. D.; Kalia, R. K.; Nakano, A.; Ramprasad, R.; Shimojo, F.; Vashishta, P. Hot-carrier dynamics and chemistry in dielectric polymers. *J. Phys. Chem. Lett.* **2019**, *10* (14), 3937–3943.
- (45) Thomas, A.; Lethuillier-Karl, L.; Nagarajan, K.; Vergauwe, R. M. A.; George, J.; Chervy, T.; Shalabney, A.; Devaux, E.; Genet, C.; Moran, J.; Ebbesen, T. W. Tilting a ground-state reactivity landscape by vibrational strong coupling. *Science* **2019**, *363* (6427), 615–619.
- (46) Wolf, T. J. A.; Sanchez, D. M.; Yang, J.; Parrish, R. M.; Nunes, J. P. F.; Centurion, M.; Coffee, R.; Cryan, J. P.; Gühr, M.; Hegazy, K.; Kirrander, A.; Li, R. K.; Ruddock, J.; Shen, X.; Vecchione, T.; Weathersby, S. P.; Weber, P. M.; Wilkin, K.; Yong, H.; Zheng, Q.; Wang, X. J.; Minitti, M. P.; Martínez, T. J. The photochemical ring-opening of 1,3-cyclohexadiene imaged by ultrafast electron diffraction. *Nat. Chem.* **2019**, *11* (6), 504–509.
- (47) Fukushima, S.; Dasgupta, N.; Kalia, R. K.; Nakano, A.; Shimamura, K.; Shimojo, F.; Vashishta, P. Photoinduced phase transition of diamond: a nonadiabatic quantum molecular dynamics study. *J. Phys. Chem. Lett.* **2025**, 9267–9272.
- (48) Wang, E.; Gupta, S.; Rafalko, C. J.; Lear, B. J.; Hickner, M. A. Structured polymer-derived ceramic composites via near-infrared thermal stereolithography. *ACS Appl. Polymer Mater.* **2025**, *7* (14), 8928–8936.
- (49) Hohenberg, P.; Kohn, W. Inhomogeneous electron gas. *Phys. Rev.* **1964**, *136* (3B), B864–B871.
- (50) Kohn, W.; Sham, L. J. Self-consistent equations including exchange and correlation effects. *Phys. Rev.* **1965**, *140* (4A), A1133–A1138.
- (51) Blochl, P. E. Projector augmented-wave method. *Phys. Rev. B* **1994**, *50* (24), 17953–17979.
- (52) Perdew, J. P.; Burke, K.; Ernzerhof, M. Generalized gradient approximation made simple. *Phys. Rev. Lett.* **1996**, *77* (18), 3865–3868.
- (53) Shimojo, F.; Fukushima, S.; Kumazoe, H.; Misawa, M.; Ohmura, S.; Rajak, P.; Shimamura, K.; Bassman Oftelie, L.; Tiwari, S. C.; Kalia, R. K.; Nakano, A.; Vashishta, P. QXMD: an open-source program for nonadiabatic quantum molecular dynamics. *SoftwareX* **2019**, *10*, 100307.
- (54) Shimojo, F.; Kalia, R. K.; Nakano, A.; Nomura, K.; Vashishta, P. Metascalable molecular dynamics simulation of nano-mechanochemistry. *J. Phys.-Condens. Matter* **2008**, *20* (29), 294204.
- (55) van Duin, A. C. T.; Baas, J. M. A.; van de Graaf, B. Delft molecular mechanics: a new approach to hydrocarbon force fields. Inclusion of a geometry-dependent charge calculation. *J. Chem. Soc. Faraday Trans.* **1994**, *90* (19), 2881–2895.
- (56) Fischer, J.; Wendland, M. On the history of key empirical intermolecular potentials. *Fluid Phase Equib.* **2023**, *573*, 113876.
- (57) Soria, F. A.; Zhang, W.; van Duin, A. C. T.; Patriot, E. M. Thermal stability of organic monolayers grafted to Si(111): insights from ReaxFF reactive molecular dynamics simulations. *ACS Appl. Mater. Interf.* **2017**, *9* (36), 30969–30981.
- (58) Berendsen, H. J. C.; Postma, J. P. M.; van Gunsteren, W. F.; DiNola, A.; Haak, J. R. Molecular dynamics with coupling to an external bath. *J. Chem. Phys.* **1984**, *81* (8), 3684–3690.